Available online at www.sciencedirect.com
SCIENCE DIRECT
International Journal of Heat and Mass Transfer 49 (2006) 427–438
International Journal of HEAT and MASS TRANSFER
www.elsevier.com/locate/ijhmt

Numerical simulations of periodic flow oscillations in low Prandtl number fluids

Daniel W. Crunkleton [1], Ranga Narayanan, Timothy J. Anderson *

Department of Chemical Engineering, University of Florida, 227 CHE, P.O. Box 11605, Gainesville, FL 32611, USA

Received 19 September 2003; received in revised form 10 September 2004
Available online 4 October 2005

Abstract

The transition from steady to oscillatory flow for a very low Prandtl number fluid ($Pr = 0.008$) is computed for rectangular enclosures with aspect ratios (length/height) of 0.25, 0.4, 1.0, and 2.0 and are found to occur at Rayleigh numbers of 250,000, 130,000, 83,500, and 30,000 respectively. The structures of the oscillations are graphically depicted and are manifested in corner cells which dissipate into centered cells and then into opposite corner cells. A secondary flow transition is detected for a geometry with an aspect ratio of 1.0 at $Ra = 1.2Ra_{c2}$.

1. Introduction

Natural convection in low Prandtl number fluids is an extremely important phenomenon in several crystal growth methods, such as the Bridgman [1–3] and Czochralski [4,5] techniques, in which a melt is condensed and solidifies into a single crystal. These techniques, however, often suffer from the disadvantage that they are adversely affected by fluid motion in the melt [6]. When the melt is heated from below, a density gradient is established and the fluid may convect in the traditional Rayleigh–Bénard fashion [7,8]. The presence of convection can significantly diminish the quality of the crystal that is produced because of morphological and compositional inhomogenities [9]; subsequently, studies of convection in its various forms have been a significant area of research.

Flow dynamics is determined primarily by the Rayleigh number, which is the ratio of the buoyant to the viscous effects and is defined as

$$Ra = \frac{g\beta\Delta T H^3}{\nu\kappa}, \tag{1}$$

where g is the gravitational acceleration, β is the thermal expansion coefficient, ΔT is the temperature difference, H is the fluid height, ν is the kinematic viscosity, and κ is the thermal diffusivity. There are three important values of the Rayleigh number which demarcate different flow bifurcations and are referred to as the first, second, and third critical Rayleigh numbers—Ra_{c1}, Ra_{c2}, and Ra_{c3}, indicating the transition to steady flow, oscillatory flow, and turbulent flow. When the Rayleigh number is below Ra_{c1}, all transport is through conduction and no convection is present. As the Rayleigh number exceeds Ra_{c1}, steady convection begins. This first critical Rayleigh number does not depend on the fluid properties (i.e., the Prandtl number) and have been studied

* Corresponding author. Tel.: +1 352 392 0882; fax: +1 352 392 9513.
E-mail addresses: tim@nersp.nerdc.ufl.edu, tim@ufl.edu (T.J. Anderson).
[1] Current Address: Department of Chemical Engineering, University of Tulsa, 600 S. College, Tulsa, OK 74104, USA.

0017-9310/$ - see front matter © 2004 Published by Elsevier Ltd.
doi:10.1016/j.ijheatmasstransfer.2004.09.009

Nomenclature

C	proportionality constant
f	frequency
g	gravitational acceleration
H	fluid height
L	length of a side being discretized ($L = 1$ for a dimensionless formulation)
Nu	Nusselt number
Pr	Prandtl number
Ra	Rayleigh number
v	dimensionless velocity (scaled by v/H)
t	dimensionless time (scaled by H^2/v)
T	dimensionless temperature (scaled by $(T - T_{\text{cold}})/(T_{\text{hot}} - T_{\text{cold}})$)
$\overline{T}$	temperature at which the Boussinesq approximation is taken ($\overline{T} = 0.5$)
ΔT	temperature difference

Greek symbols

β	thermal expansion coefficient
γ	aspect ratio (scaled to H)
κ	thermal diffusivity
v	kinematic viscosity

Subscripts

c1	first critical Rayleigh number
c2	second critical Rayleigh number
c3	third critical Rayleigh number

extensively by several authors using both linear stability arguments [10–13] and numerical CFD codes [14,15].

When studying Ra_{c2}, however, many previous numerical studies have been limited to two-dimensional enclosures. For example, Ozoe and Hara [16] characterize the transition to periodic oscillations in fluids of $Pr = 0.01$ in two-dimensional rectangular enclosures of aspect ratio (length/height) of 4.0 using a finite-difference method. Once convection begins, the calculated oscillations manifested themselves in the form of multiple convection cells that deform as time progressed. They also conclude that the difference between the first and second critical Rayleigh numbers decrease as the Prandtl number decreases. Two-dimensional studies of the transition to oscillatory flow, however, often oversimplify the rich convection which may be present, especially those in rectangular enclosures, which are influenced by the presence of corners which in turn affect the flow patterns. Three-dimensional convection cells, whether oscillatory or not, often have vortices in the corners of the domains [15], and this effect cannot be reproduced as well as with two-dimensional algorithms; therefore a three-dimensional numerical study is needed to properly determine the second critical Rayleigh number.

One of the few three-dimensional numerical studies of natural convection of low-Prandtl-number fluids was performed by Neumann [17]. This study considered the natural convection of low-Prandtl-number fluids ($Pr = 0.02$) in vertical circular cylinders heated from below, in both steady and periodic oscillatory regimes. The results show that in the steady regime, multiple steady states are possible under similar conditions, depending on the past history of the fluid. This work did resolve the fundamental process of oscillation in low Prandtl number liquids from that observed in gases; namely, oscillations of gases in cylindrical enclosures are accompanied by the rotation of the plane of symmetry about the axis of the cylinder, while in liquids it involves spatial changes in the flow structure.

In this study, the second critical Rayleigh numbers will be computed numerically for liquid tin ($Pr = 0.008$). Tin is taken as the model fluid primarily because it has an extremely low Prandtl number. Several researchers [18–20], including the authors [21], are developing new techniques for detecting convection in crystal growth. Such techniques must be tested and applied to low Prandtl number fluids that are encountered in crystal growth. This work is intended to provide a numerical comparison for these studies, based on one of the lowest Prandtl number fluids available.

The following rectangular aspect ratios are investigated: 0.25, 0.4, 1.0, and 2.0. As mentioned earlier, the presence of corners in rectangular enclosures is known to add more complexity and three-dimensionality to any buoyancy-driven flows [15], when compared with cylindrical geometries. As experimental techniques for detecting convection in low Prandtl number fluids are developed, very robust tests will be required and the corners in rectangular geometries will allow this.

2. Algorithm

A three-dimensional, finite-volume algorithm developed and tested previously [15] was used for all calculations. The following Boussinesq equations are solved

$$\begin{aligned} &\nabla \cdot \vec{v} = 0, \\ &\frac{\partial \vec{v}}{\partial t} + \vec{v} \cdot \nabla \vec{v} = -\nabla p + \nabla^2 \vec{v} - \frac{Ra}{Pr}(T - \overline{T})\vec{k}, \\ &Pr\left(\frac{\partial T}{\partial t} + \vec{v} \cdot \nabla T\right) = \nabla^2 \mathrm{T}, \end{aligned} \tag{2}$$

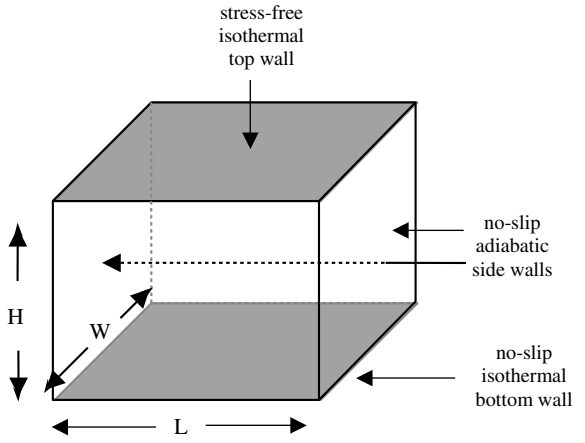

Fig. 1. Geometry and boundary conditions studied in this work.

where the scales for velocity, time, and temperature are (ν/H), (H^2/ν), $(T - T_{\text{cold}})/(T_{\text{hot}} - T_{\text{cold}})$ respectively, and $\overline{T}$ is the temperature at which the Boussinesq properties are taken, ($\overline{T} = 0.5$ in this study). The geometry and boundary conditions are shown in Fig. 1. These equations are discretized in space with a piecewise linear profile and discretized in time using a fully implicit scheme. The velocity profiles were made to satisfy the continuity equation using the SIMPLE pressure correction algorithm (semi-implicit method of pressure linking equations). The calculations were taken as converged if the difference between successive iterations scaled to the final values was less than or equal to 10^{-9}. For more details into the specifics of the technique, readers are referred to the book of Patankar [22], which details the procedures.

When first critical Rayleigh numbers are calculated, the specific value of Ra_{c1} can be calculated through a Nusselt number averaged over the active surfaces, noting that $Ra \to Ra_{c1}$ as $Nu \to 1$; there is, however, no analogous test for the second critical Rayleigh number. For this study, the second critical Rayleigh number was isolated by noting the velocity components and dimensionless temperature at a pre-selected point to see if periodic oscillations develop. If, for that Rayleigh number, no oscillations are detected, its velocity and temperature results are used as initial guesses for the next calculation, with an increased Rayleigh number. This process in repeated until oscillations are detected, and the lowest Rayleigh number at which oscillations are detected is taken as the second critical Rayleigh number. For some initial calculations, additional simulations were performed for higher Ra, and the amplitudes of the oscillations were noted, and the value of Ra at which the amplitudes extrapolated to zero was taken to be Ra_{c2}. This procedure, however, did not yield Ra_{c2} values that were statistically different from simple trial and error, so it was not used afterwards.

For all calculations, a staggered grid structure was used which placed more data points along the sides and corners of the enclosure and less in the interior. This was done to ensure resolution of side and corner effects which are important in rectangular geometry studies. To do this, the following equations were used to form the grid:

$$X_i = X_{i-1} + \Omega \sin\left(\frac{i\pi}{N+1}\right), \tag{3}$$

where X indicates the grid point, N is the number of grid points in the appropriate direction, the subscript i indicates the desired grid point and $i-1$ is the location of the previous grid point. The function Ω is defined as

$$\Omega = \frac{L}{\sum_{i=1}^{N} \sin\left(\frac{i\pi}{N+1}\right)}, \tag{4}$$

where L is the length of the side being discretized. Eqs. (3) and (4) allow additional grid points to be placed at the periphery of the enclosure to allow greater resolution of the corner effects.

Different mesh sizes were used for different aspect ratios, and are given as each aspect ratio is presented in Section 3. As the Ra_{c2} calculations began for a given aspect ratio, the converged steady (Ra_{c1}) profile was used as the initial guess, and the Ra_{c2} calculation proceeded as indicated before. Therefore, the same mesh sizing was used for the Ra_{c1} and Ra_{c2} profiles. The meshes that were actually chosen in the Ra_{c1} calculation were the finest that could be used in the computers available. No additional calculations with finer or coarser grids were used.

3. Results and discussion

The results obtained for Ra_{c1} and Ra_{c2} are shown in the stability diagram in Fig. 2. In this figure, the trend of the computed Ra_{c1} values agrees well with the linear stability results of Chandrasekhar [11] for an infinite aspect ratio and Catton [10] for finite aspect ratios. The Ra_{c1} results compare favorably with the numerical result of Ozoe et al. [23]. The computed Ra_{c2} values also compare well with other calculations performed for similar problems. The Ra_{c2} trend of this work, for example, is consistent with the two-dimensional result of Ozoe and Hara [16] for $\gamma = 3$ and $\gamma = 4$ (for $Pr = 0.01$) and the three-dimensional work of Nakano et al. [24] for $\gamma = 5$ and $Pr = 0.1$.

The Ra_{c2} results from this study can also be checked against the theoretical predictions of Busse [25] who predicts that as $Pr \to 0$, the frequency of oscillations are related to the Rayleigh number through

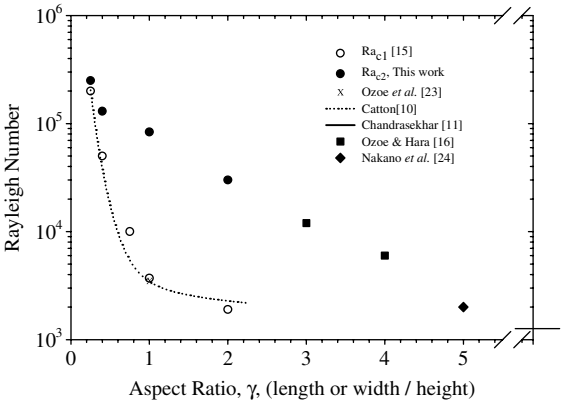

Fig. 2. Calculated first (Ra_{c1}) and second (Ra_{c2}) critical Rayleigh numbers for liquid tin ($Pr = 0.008$).

$$f = C\left(\frac{Ra - Ra_{c1}}{Ra_{c1}}\right)^{\frac{1}{2}}, \tag{5}$$

where C is a constant. The flow profiles corresponding to the Ra_{c2} points in Fig. 2 will be detailed in a later section; however, if their fundamental frequencies of oscillation are calculated using a fast Fourier transform and the results analyzed with a least squares regression, a linear fit with $R^2 = 0.97$ and a slope of $C = 0.0303$ Hz is obtained. This compares favorably with the experimental results of Mishra et al. [26] in which $C = 0.022$ Hz is obtained.

As seen in Fig. 2, Ra_{c2} does not appear to be as sensitive to aspect ratio as Ra_{c1}. The physical explanation for this is not obvious; it is hypothesized that since the Ra_{c1} transition involves the fluid overcoming the inertia to a convective state means that the buoyancy leading to this steady convection must build over the entire vertical distance of the fluid geometry. Thus, the Ra_{c1} transition would depend more on this distance (i.e., γ) than the Ra_{c2} transition. For the Ra_{c2} transition, the fluid is already convecting and the result of the transition is simply to change the manner in which the fluid moves. This would have less to do with geometry than the original Ra_{c1} transition.

The results obtained for each individual aspect ratio are summarized in Table 1 and are detailed in the next sections. The validity of the results to be presented can be substantiated quantitatively by the Busse test outlined above. Additionally, qualitative substantiation is provided by noting that that oscillations in low Prandtl number fluids are expected to be oscillations of the convective cell shape as opposed to periodic changes in the velocity direction and/or magnitude [17]. In the results that follow, the former is observed.

Table 1
Summary of oscillatory convection results for $Pr = 0.008$

Aspect ratio, γ	Grid	Calculated Ra_{c2}	Comments about oscillations
0.25	$20 \times 20 \times 30$	250,000	Center → corner → center
0.4	$20 \times 20 \times 30$	130,000	Center → corner → center. Extremely subtle
1	$25 \times 25 \times 25$	83,500	Corner cells oscillation between circular- and cigar-shaped. Very subtle
2	$30 \times 30 \times 20$	30,000	Not periodic oscillations

3.1. $\gamma = 0.25$

Simulations carried out for $\gamma = 0.25$ in the supercritical Rayleigh number regime captured some of the rich

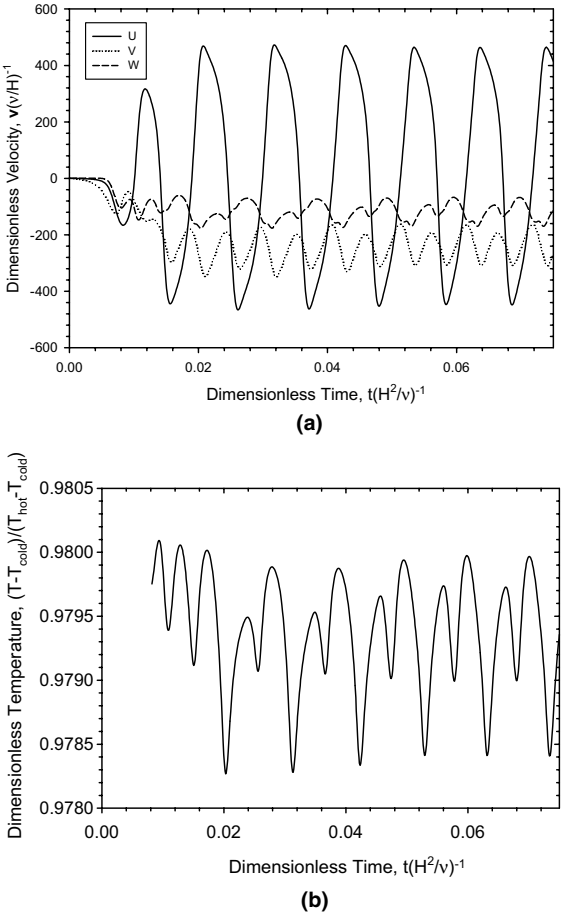

Fig. 3. Periodic oscillations for $Ra = 250{,}000$ and $\gamma = 0.25$: (a) dimensionless velocity and (b) dimensionless temperature. The tracking point is in the center is the container at the grid point nearest to 10% of the distance from the bottom.

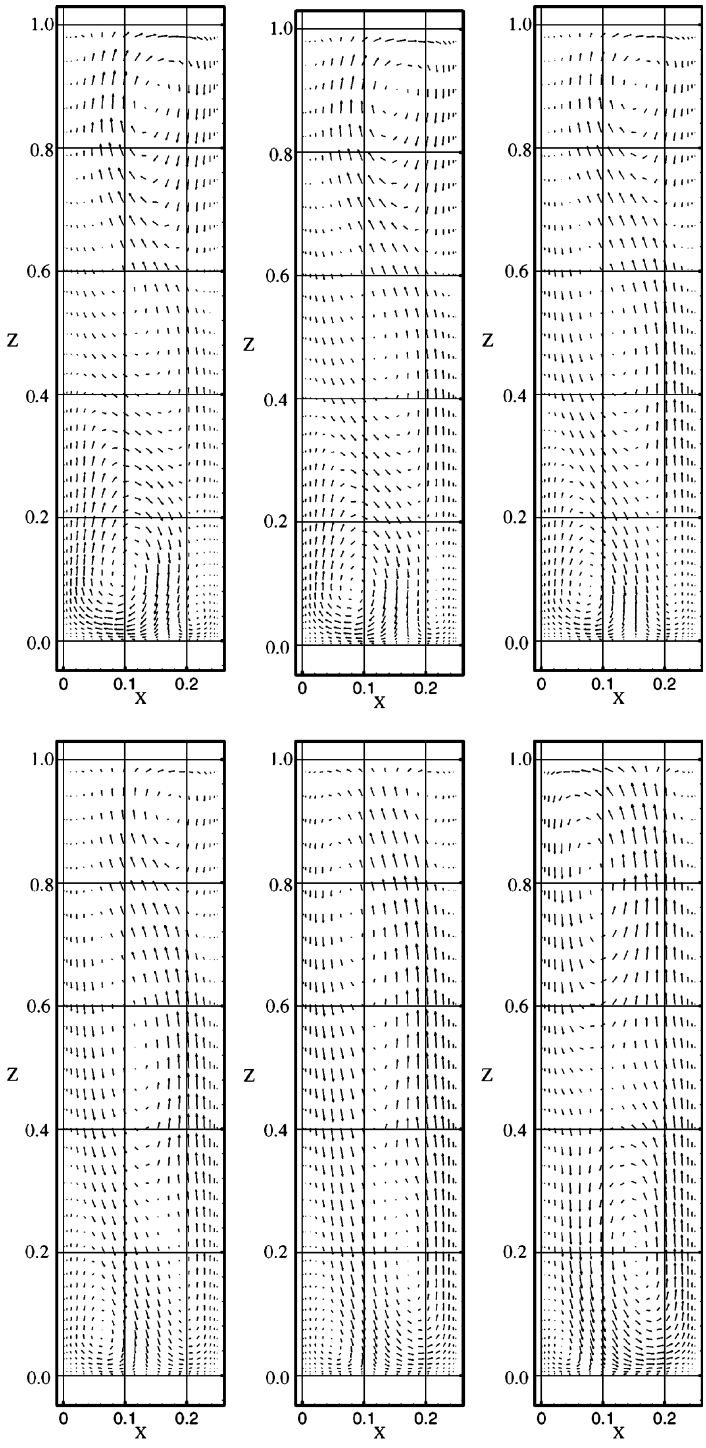

Fig. 4. Flow evolution of oscillatory flow with $Ra = 400{,}000$, $Pr = 0.008$, $\gamma = 0.25$. The time step is 2.5×10^{-4} in dimensionless units. If the fluid height is assumed to be 1.5 cm, this corresponds to a time step of 0.25 s.

dynamics of oscillatory flow in low-Prandtl-number fluids. Using a $20 \times 20 \times 30$ rectangular grid, oscillatory convection starts at a Rayleigh number (Ra_{c2}) of 250,000, which is relatively close to the first critical

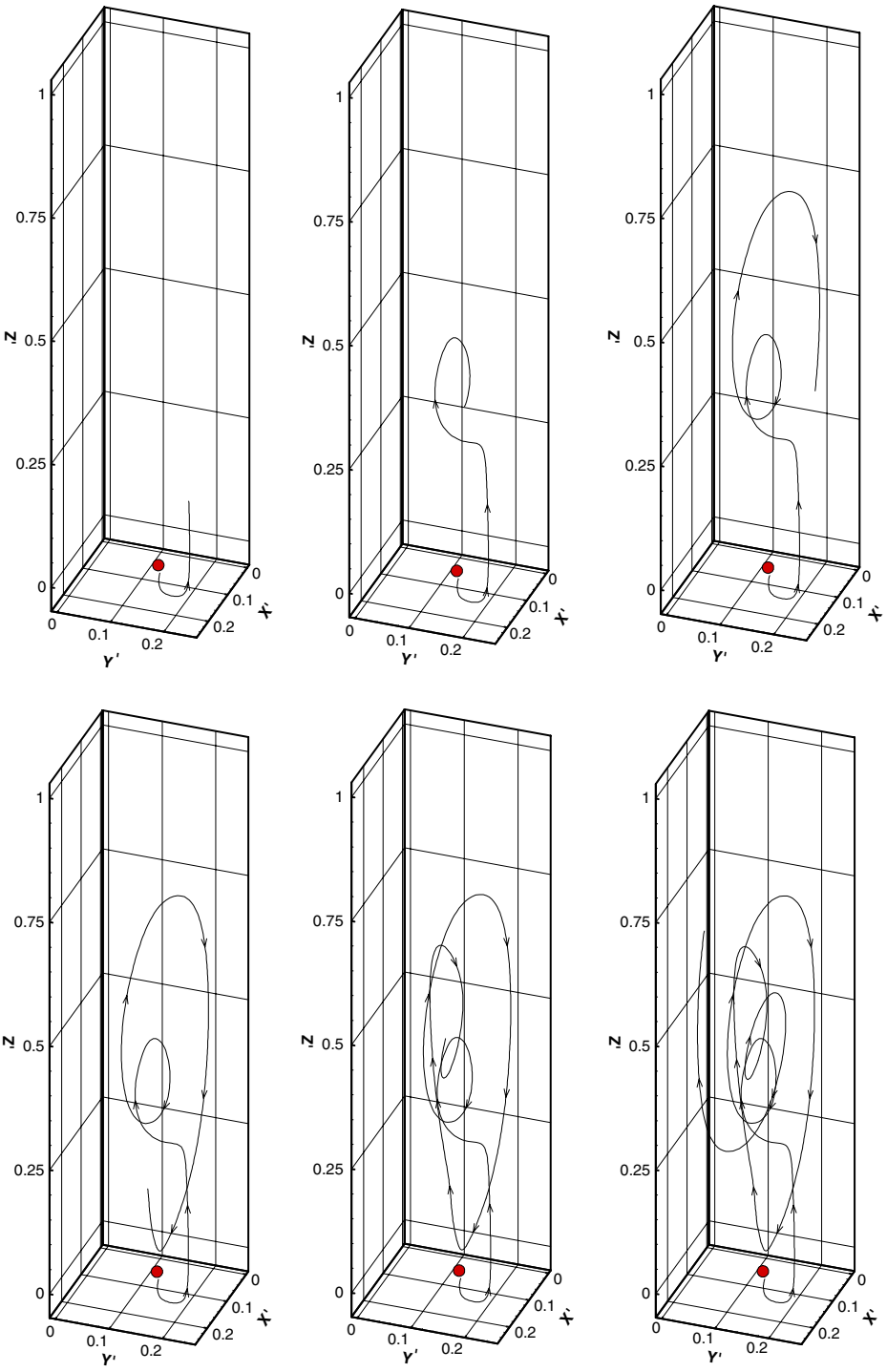

Fig. 5. Streamline trace of quasi flow profile for $Ra = 400{,}000$, $Pr = 0.008$, $\gamma = 0.25$. The flow chosen is a snapshot of Fig. 4 and the streamline is integrated over length in the domain.

Rayleigh number ($Ra_{c1} = 200{,}000$), a result observed experimentally by Müller et al. [27] for liquid gallium in tall cylindrical enclosures. Fig. 3 shows the oscillatory nature of this flow using a time step of 5×10^{-5} in

dimensionless units at a point in the center of the flow at the grid point nearest to 10% of the vertical distance from the bottom.

To visualize the intricacies of the flow oscillations, Fig. 4 shows the oscillatory patterns the fluid makes in the x–z plane with a time step of 2.5×10^{-4}. (If a fluid height of 1.5 cm is assumed, this corresponds to a time step of 0.34 s.) In the first three frames, there is not as much change in the overall flow pattern as in the final three. The changes that do occur are manifested in the velocity magnitudes, and in the bottom-left cell which becomes slightly more circular. Additionally, the cell in the top right of the domain moves upward slightly and becomes more compact in frame (c). Also in frame (c), a large cell in the center of the flow field begins to form. In frame (d), the cell formed in the center is evident, and in (e), it dominates the flow field, with only a secondary vortex in the lower left corner. Finally, in frame (f), the center cell has divided into two smaller cells—in the upper left and bottom right, approximately a mirror-image of frame (a). In general, the oscillations can be thought of as a series of the following steps:

1. Begin with two cells in opposite corners.
2. Slowly transform the corner cells to a single, central vortex that is diagonally skewed.
3. Quickly transform the center cell into two cells in the opposite corners of (1).
4. Repeat.

It should be mentioned that the orthogonal (yz) plane was also similarly analyzed and flow oscillations were manifested through a single, diagonally skewed cell whose diameter oscillates. This flow structure, however, could not be easily visualized in a two dimensional graph because the magnitude of these oscillations were small.

The structure of the oscillations for the first quasi-steady state profile in Fig. 4 is shown in Fig. 5. The cellular pattern is obvious; yet it is also clear that the flow streamline is highly three-dimensional (and does not close). The flow pattern is actually more helical than it is cellular.

3.2. $\gamma = 0.4$

Using the converged Ra_{c1} profiles for this aspect ratio as an initial guess and a $20 \times 20 \times 30$ grid, a Ra_{c2} value of 130,000 was obtained and the resulting velocity and temperature oscillations for this Rayleigh number are shown in Fig. 6. As seen in this figure, the behavior of the velocity components is much more complex than those for $\gamma = 0.25$, while the temperature oscillations are much simpler. For $\gamma = 0.25$, the x-component of velocity (i.e., u) dominated the oscillations, while for $\gamma = 0.4$, the y-component (i.e., v) is greater.

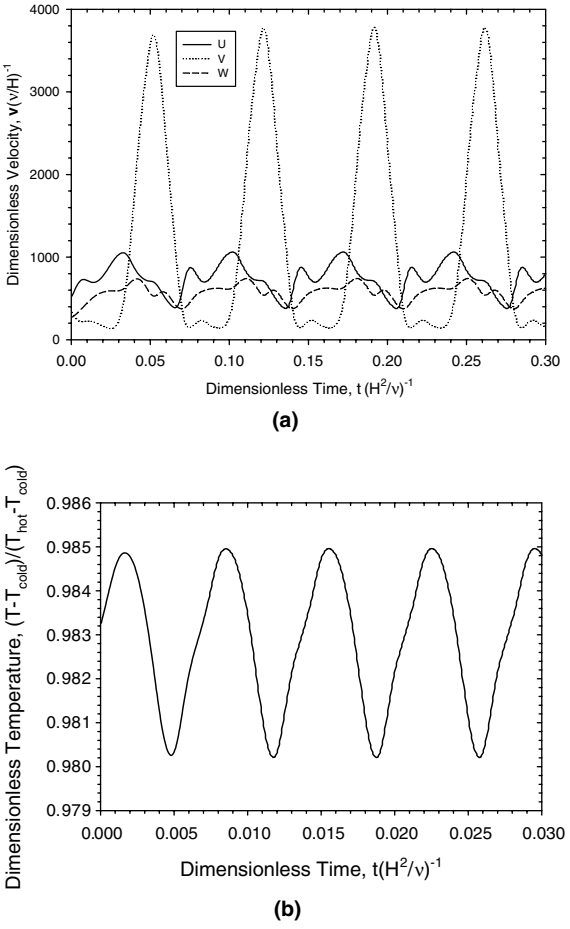

Fig. 6. Flow oscillations for $Ra = 130{,}000$, $\gamma = 0.4$: (a) dimensionless velocity and (b) dimensionless temperature. The tracking point is in the center is the container at the grid point nearest to 10% of the distance from the bottom.

A macroscopic flow pattern of these oscillations was constructed and is shown in Fig. 7. Both the magnitude of the flow velocity and the translation of the convective cells in the domain occurred over shorter time scales than for $\gamma = 0.4$ than for $\gamma = 0.25$. For this reason, the individual frames in Fig. 7 are for a finer time spacing of 4×10^{-5} (if $H = 1.5$ cm, this corresponds to 0.06 s). The flow begins in (a) with two nearly circular cells in the bottom right and upper left, with a smaller, cigar-shaped cell in the bottom left. There is a larger cell, diagonally skewed near the center of the domain. As frame (b) is reached, the lower right cell has shrunk, while the lower left has grown, although their circular and cigar shape has been preserved. The formation of the center cell has completed and is now vertical in the domain. The upper left cell has shrunk and the beginning of an upper right cell is evident. In frame (c), the upper right cell formation has completed, and on the lower left boundary, a

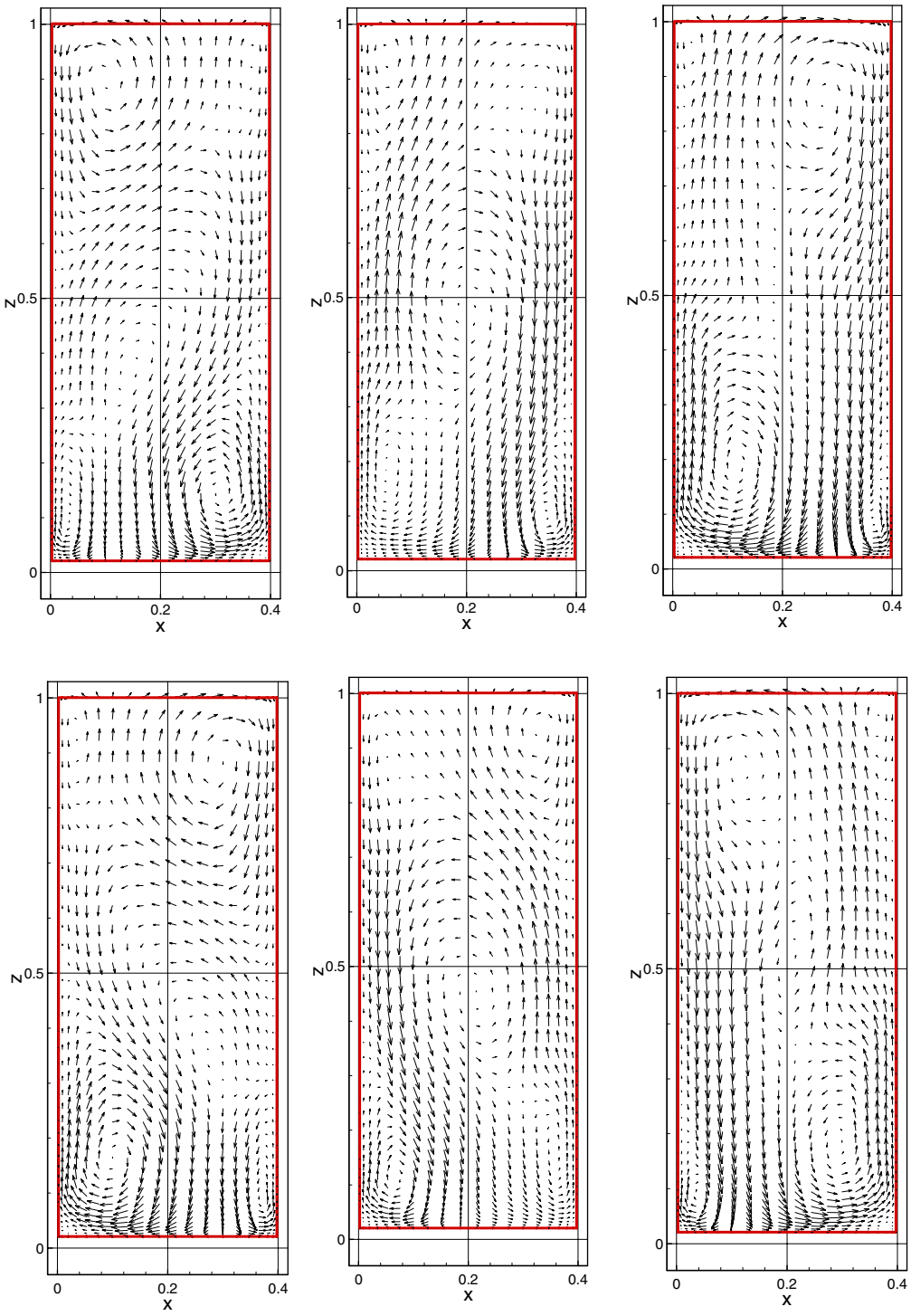

Fig. 7. Flow visualization for $Ra = 130{,}000$, $Pr = 0.008$, and $\gamma = 0.4$. The time step is 4×10^{-5}, which corresponds to 0.06 s if $H = 1.5$ cm.

large cell with a much smaller vortex on the right is seen. Frames (d), (e), and (f) are practically mirror images of (a), (b), and (c). The results obtained from $\gamma = 0.25$ and $\gamma = 0.4$ suggest flow oscillations for these geometries

manifest themselves in low-Prandtl-number fluids in the same qualitative pattern—by the shifting of corner vortices, to a centered cells, and then to vortices in the opposite the corners.

3.3. $\gamma = 1.0$

The second critical Rayleigh number for an enclosure with an aspect ratio of 1.0 and a $25 \times 25 \times 25$ grid, was determined to be 83,500. A trace of the velocity components and dimensionless temperature for $Ra = 85{,}000$ are shown in Fig. 8, showing definite periodicity. When analyzing the macroscopic nature of this flow configuration, changes of the cellular structure were confined to the corners of the domain and oscillate between a circular and a cigar-shaped configuration. This effect is very subtle and cannot be easily visualized in a manner similar to Figs. 4 or 7.

Although a macroscopic analysis of the flow oscillations was not possible for this aspect ratio, an interesting phenomenon was observed when the Rayleigh number is increased even further beyond Ra_{c2} that was not observed for the smaller aspect ratio enclosures. If, for $\gamma = 1.0$, the Rayleigh number is increased beyond Ra_{c2} (as seen in Fig. 9a through d), a secondary transition is observed beginning at $Ra = 100{,}000$. Additionally, if the fundamental frequencies of oscillation for $Ra = 85{,}000$ and $Ra = 100{,}000$ are calculated using the fast Fourier transform, the fundamental frequency shifts for all velocity components. The amount of this shift is approximately constant for all velocity components, at a value of 0.036 Hz (assuming a fluid height of 1.5 cm). As far as the authors are aware, this secondary oscillation has not been observed in previous experimental or computational studies and experiments are underway to verify these observations.

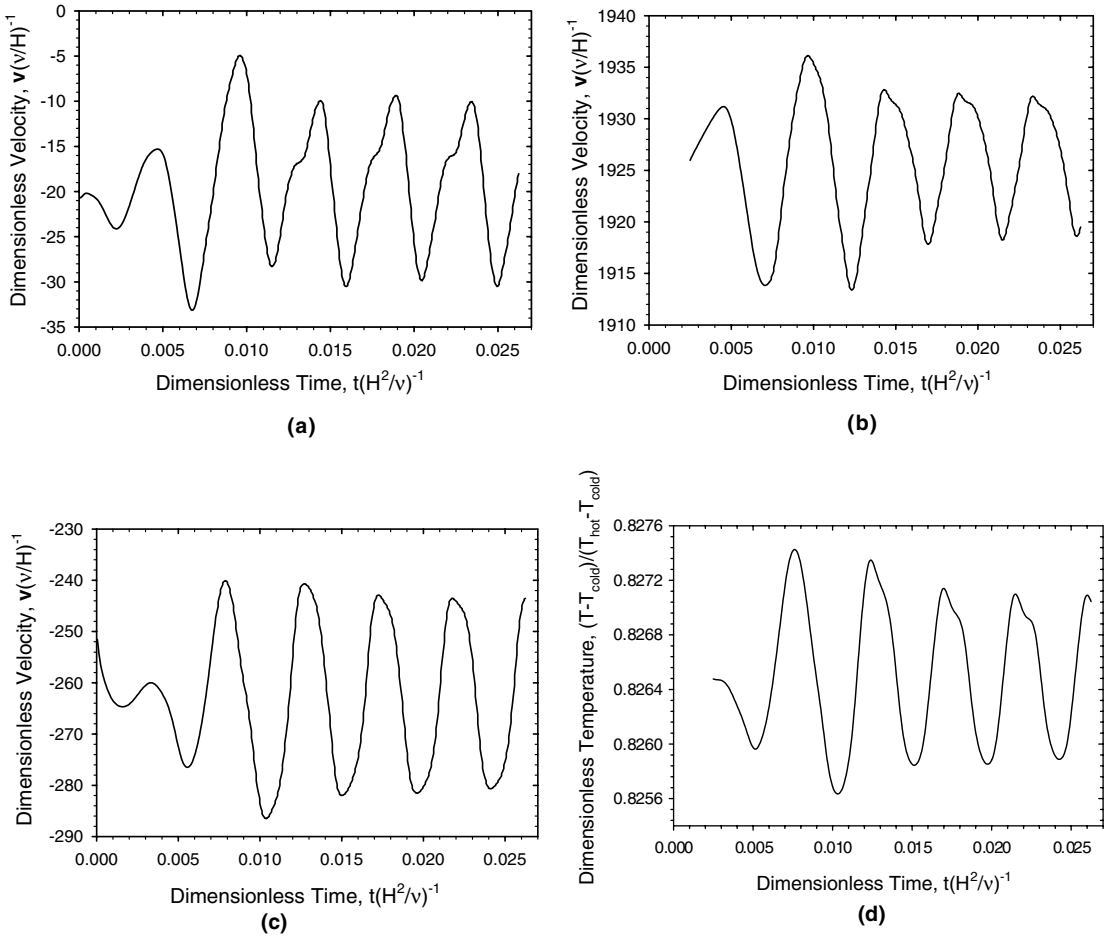

Fig. 8. Periodic oscillations for $Ra = 85{,}000$ and $\gamma = 1.0$: (a) X-component, (b) Y-component, (c) Z-component and (d) dimensionless temperature.

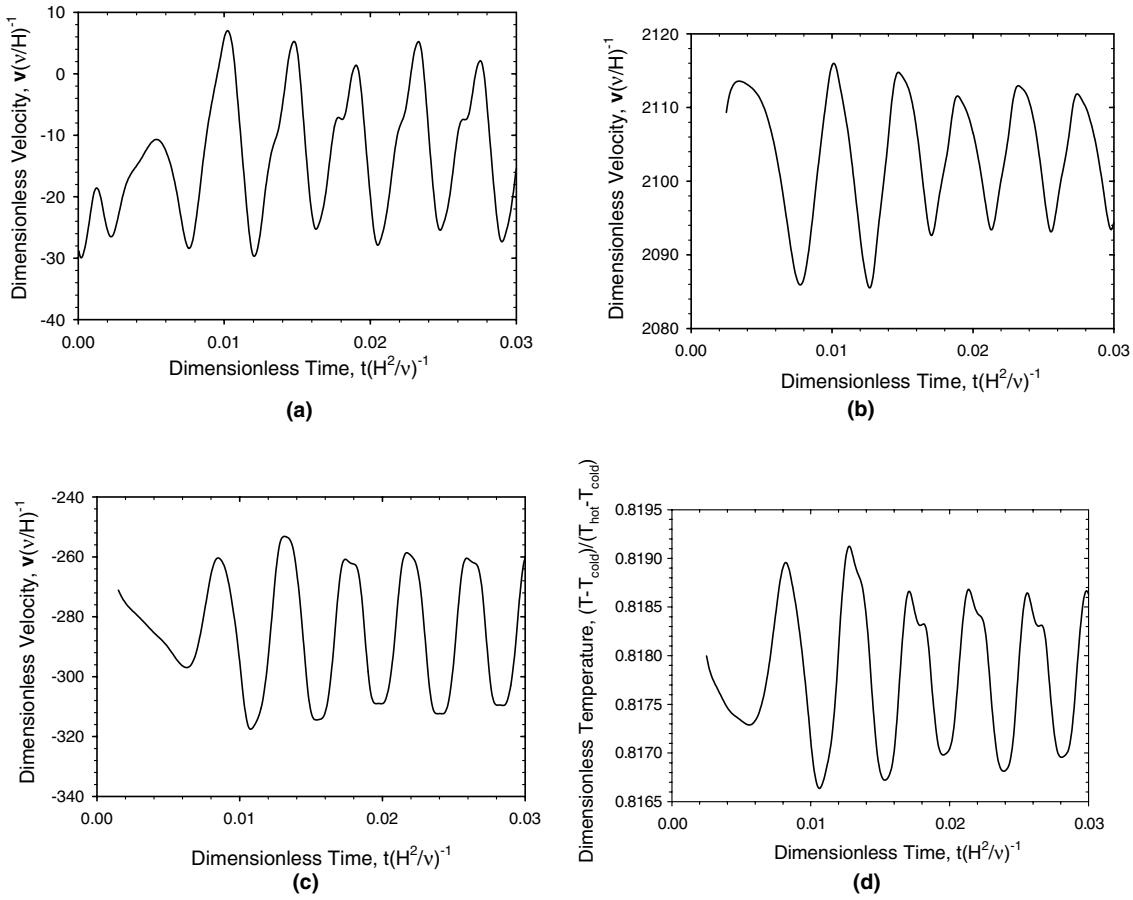

Fig. 9. Development of secondary oscillations in $Ra = 100{,}000$, $\gamma = 1.0$: (a) X-component, (b) $Y =$ component, (c) Z-component and (d) dimensionless temperature.

3.4. $\gamma = 2.0$

Using the steady-state velocity and temperature profiles for the Ra_{c1} previously determined to be 1800, and with a $30 \times 30 \times 20$ grid, oscillations for this aspect ratio began at a Ra_{c2} of 30,000. Fig. 10 shows the oscillations that were detected; however, these oscillations, unlike those of lower aspect ratios, were not periodic. Several modifications to the relaxation parameters of the algorithm were made, but the same result was obtained. A similar non-periodic oscillations was observed computationally by Ozoe and Hara [16] for two-dimensional calculations.

4. Summary

The following second critical Rayleigh numbers were obtained for a fluid with $Pr = 0.008$: 250,000 for $\gamma = 0.25$; 130,000 for $\gamma = 0.4$; 83,000 for $\gamma = 1.0$; and 3000 for $\gamma = 2.0$. For the $\gamma = 0.25$ and 0.4 cases, the flows oscillate by corner cells moving back and forth across the xz plane. For $\gamma = 1.0$, corner cells changed from circular to cigar shaped, but in a very subtle fashion. For $\gamma = 1.0$ and $Ra = 1.2Ra_{c2}$, a secondary transition was observed that slightly deformed the shape of the oscillations and changed the fundamental frequency of oscillation by 0.036 Hz. Finally, non-periodic flows were observed for $\gamma = 2.0$. All computed results obtained compared favorably with previous experiments using a mathematical test developed by Busse [25].

Acknowledgements

This work was supported through NASA grant NAG8-1243 and the Graduate Student Research Program.

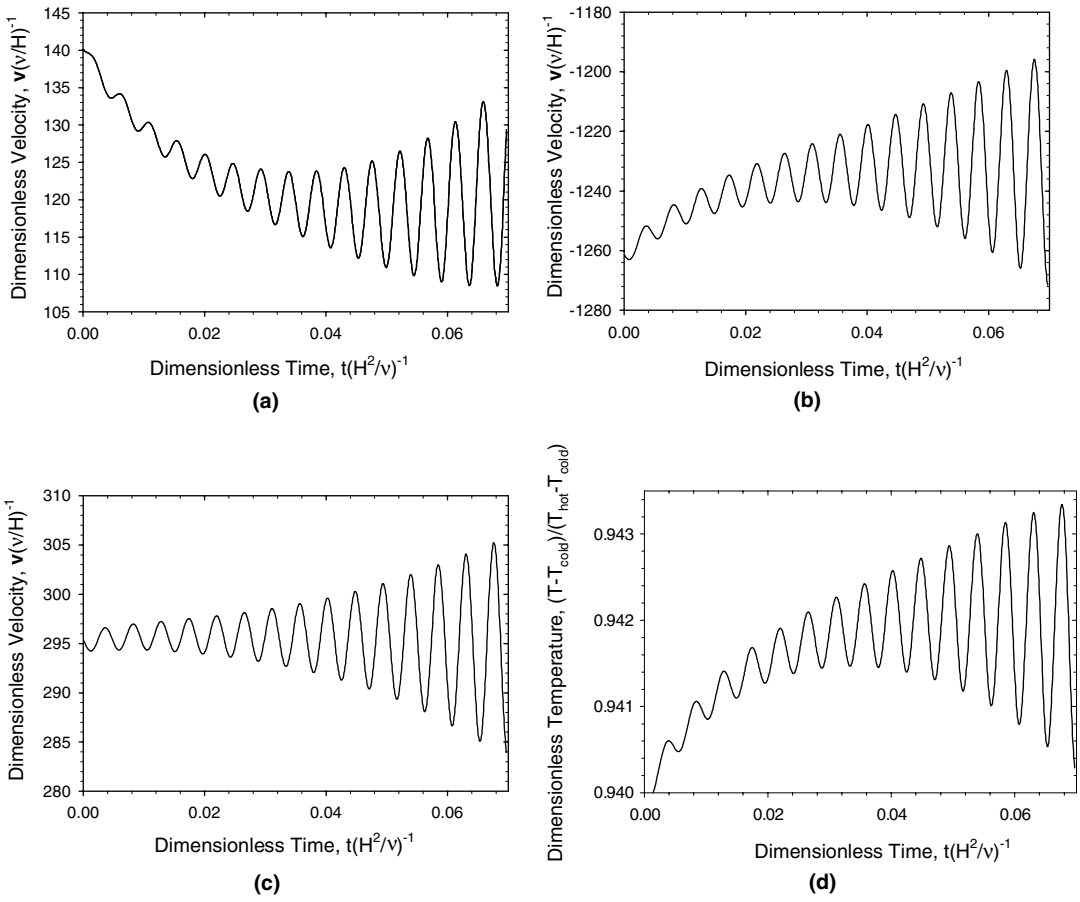

Fig. 10. Non-periodic oscillations for $Ra = 30{,}000$ and $\gamma = 2.0$: (a) X-component and (b) Y-component.

References

[1] P.W. Bridgman, Proc. Am. Acad. Arts Sci. 60 (1925) 305–315.

[2] J.J. Favier, Recent advances in Bridgman growth modeling and fluid flow, J. Cryst. Growth 99 (1990) 18–29.

[3] A.W. Vere, Crystal Growth: Principles and Progress, Plenum, New York, 1987, pp. 79–82.

[4] J. Czochralski, Ein neunes Vefahren zur messung der Kristallisationsgeschwindigkeit der Metalle, Z. Phys. Chem. 92 (1918) 219–221.

[5] V. Prasad, H. Zhang, A.P. Anselmo, Transport phenomena in Czochralski crystal growth processes, in: J.P. Harnett, T.F. IrvineJr. (Eds.), Advances in Heat Transfer, Academic Press, San Diego, 1997, pp. 313–435.

[6] A.W. Vere, Crystal Growth: Principles and Progress, Plenum, New York, 1987, pp. 67–88.

[7] M.H. Bénard, Les toubillions cellulaires dans une nappe liquide transportant de la chaleur par convection en régime permanente, Ann. Chem. Phys. 23 (1901) 62–144.

[8] L. Rayleigh, On convective currents in a horizontal layer of fluid when the higher temperature in on the underside, Philos. Mag. 32 (1916) 529–546.

[9] I. Nicoara, M. Nicolov, A. Pusztai, D. Vizman, On the solidification particularities of the opaque and semi-transparent crystals obtained by Bridgman method, Cryst. Res. Technol. 33 (1998) 207–218.

[10] I. Catton, The effect of insulating vertical walls on the onset of motion in a fluid heated from below, Int. J. Heat Mass Transfer 15 (1972) 665–672.

[11] S. Chandrasekhar, Hydrodynamic and Hydromagnetic Stability, Dover, New York, 1961, pp. 9–75.

[12] G.S. Charlson, R.L. Sani, Thermoconvective instability in a bounded cylindrical fluid layer, Int. J. Heat Mass Transfer 13 (1970) 1479–1496.

[13] G.S. Charlson, R.L. Sani, On thermoconvective instability in a bounded cylindrical fluid layer, Int. J. Heat Mass Transfer 14 (1971) 2157–2160.

[14] M.P. Arroyo, J.M. Saviron, Rayleigh–Bénard convection in a small box: spatial features and thermal dependence of the velocity field, J. Fluid Mech. 235 (1991) 325–348.

[15] D.W. Crunkleton, N. Gupta, R. Narayanan, T. Anderson, Natural convection of low-Prandtl-number fluids in rectangular enclosures, AIAA Technical Paper 99-0840, 1999.

[16] H. Ozoe, T. Hara, Numerical analysis for oscillatory natural convection of low Prandtl number fluid heated

from below, Numer. Heat Transfer Part A 27 (1995) 307–317.
[17] G. Neumann, Three-dimensional numerical simulation of buoyancy-driven convection in vertical cylinders heated from below, J. Fluid Mech. 214 (1990) 559–578.
[18] J.N. Koster, Visualization of Rayleigh–Bénard convection in liquid metals, Eur. J. Mech. B—Fluids 16 (1997) 447–454.
[19] K. Kakimoto, Flow instability during crystal growth from the melt, Prog. Cryst. Growth Charact. Mater. 30 (1995) 191–215.
[20] K. Kakimoto, M. Eguchi, H. Watanabe, T. Hibiya, Direct observation by X-ray radiography of convection of molten silicon in the Czochralski growth method, J. Cryst. Growth 88 (1988) 365–370.
[21] S.R. Prasad, C. Malika, T.J. Anderson, R. Narayanan, An electrochemical method to detect flow profiles during convection in liquid metals, J. Cryst. Growth 198/199 (1999) 194–200.
[22] S.V. Patankar, Numerical Heat Transfer and Fluid Flow, Hemisphere, Washington, 1980, pp. 126–131.
[23] H. Ozoe, K. Yamamoto, S.W. Churchill, H. Sayama, Three-dimensional, numerical analysis of laminar convection in a confined fluid heated from below, J. Heat Transfer 98 Ser C (Ser C) (1976) 202–207.
[24] A. Nakano, H. Ozoe, S.W. Churchill, Numerical computation of natural convection for a low Prandtl-number fluid in a shallow rectangular region heated from below, Chem. Eng. J. 71 (1998) 175–182.
[25] F. Busse, The oscillatory instability of convection rolls in a low Prandtl-number fluid, J. Fluid Mech. 52 (part 1) (1972) 97–112.
[26] D. Mishra, K. Muralidhar, P. Munshi, Isotherms in a horizontal differentially heated cavity at intermediate Rayleigh numbers, Int. Commun. Heat Mass Transfer 26 (1999) 729–738.
[27] G. Müller, G. Neumann, W. Weber, Natural convection in vertical Bridgman configurations, J. Cryst. Growth 70 (1984) 78–93.